ORBITING IN COLLISIONS BETWEEN LIGHT HEAVY IONS ($A_T + A_p < 50$)

D. Shapira, K. A. Erb, J. L. C. Ford, Jr., J. Gomez del Campo,
B. Shivakumar[*], R. Novotny,[†] and D. Schull[**]
Oak Ridge National Laboratory[††], Oak Ridge, Tennessee 37830

S. T. Thornton, R. L. Parks and R. Cecil
Physics Department, University of Virginia
Charlottesville, Virginia 22901

ABSTRACT

Evidence is presented for the formation of a long-lived rotating
dinuclear complex in the early stages of the collision between light
heavy nuclei. A study of the variation of the total kinetic energy of
the outgoing fragments with bombarding energy allows a determination of
the average dinuclear separation prior to scission. At higher bombarding
energies the study reveals that the system of the two colliding nuclei
has reached a critical value of angular momentum beyond which it can not
be trapped into an orbiting configuration.

All references to orbiting in this work are to a process wherein colliding nuclei form a rotating dinuclear complex. Only part of the projectile's initial kinetic energy is stored in the relative dinuclear motion (nuclear, Coulomb and centrifugal energies) and the remainder of the initial kinetic energy goes into internal excitation of both fragments (Fig. 1). When the nuclei r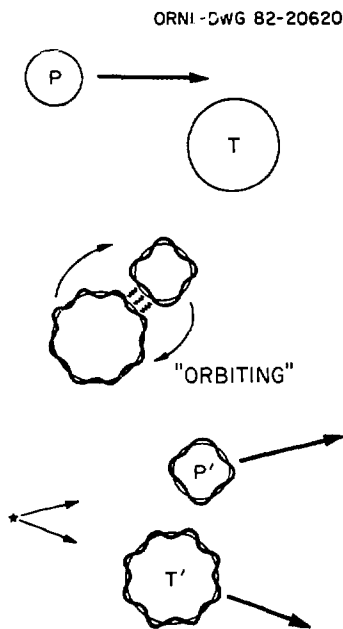eseparate only that part of the initial kinetic energy which was stored in the relative dinuclear motion appears as kinetic energy of the final fragment (generally referred to as the complete damping of the projectile's kinetic energy). The formation of a short-lived dinuclear system was postulated long ago in connection with deep inelastic collisions seen in heavier systems.[1] We have gathered a large body of data[2-5] that, together with data from other laboratories,[6,7] shows that the formation of a long-lived rotating dinuclear system is a general process occurring in the interaction between light heavy ions.

ORNL-DWG 82-20620

"ORBITING"

FIG. 1. Orbiting of nuclei — a schematic presentation.

Data showing the effects under consideration were taken for the $^{20}Ne + ^{12}C$,[2] $^{20}Ne + ^{20}Ne$[3] and $^{28}Si + ^{12}C$[4] systems, and also for the non α conjugate systems $^{27}Al + ^{16}O$[5] and $^{29}Si + ^{12}C$. The most complete data,

however, were obtained for ^{28}Si + ^{12}C and the ensuing discussion will focus mainly on these data, measured at the Brookhaven National Laboratory and Oak Ridge National Laboratory Tandem Accelerators.

A large part of the data to be presented are inelastic and few nucleon transfer reaction products from the scattering of ^{12}C on ^{28}Si measured at backward angles (close to 180°) over a wide energy range. In th experiment a ^{12}C target is bombarded with a ^{28}Si beam and all the recoiling target-like products are measured at forward angles. The ^{12}C nuclei recoiling to forward angles correspond to the backscattering of C from a Si target, but provide the advantage of high kinetic energies and forward focusing of the reaction products of interest. The experimental setup is shown in Fig. 2. For the purpose of measuring target-like products recoiling to very forward angles a gas filled absorber was placed in front of the ΔE-E position sensitive telescope. At each bombarding energy the absorber pressure was adjusted to stop the scattered ^{28}Si projectiles as well as any heavier products: the lighter target-like products penetrated the absorber without losing a significant fraction of their recoil kinetic energy. Figure 3 illustrates the quality and nature of the data acquired with this method. Two dimensional ΔE-E spectra measured at the same scattering angle and the same bombarding energy with and without the absorber in front of the counter are compared. It can be easily seen that with the exception of the particles recoiling with very low energy the entire dynamic range of recoil energies is measured for boron, carbon, nitrogen and oxygen. Figure 4 shows energy spectra for ^{12}C measured simultaneously at five angles over a 10° range subtended by the position
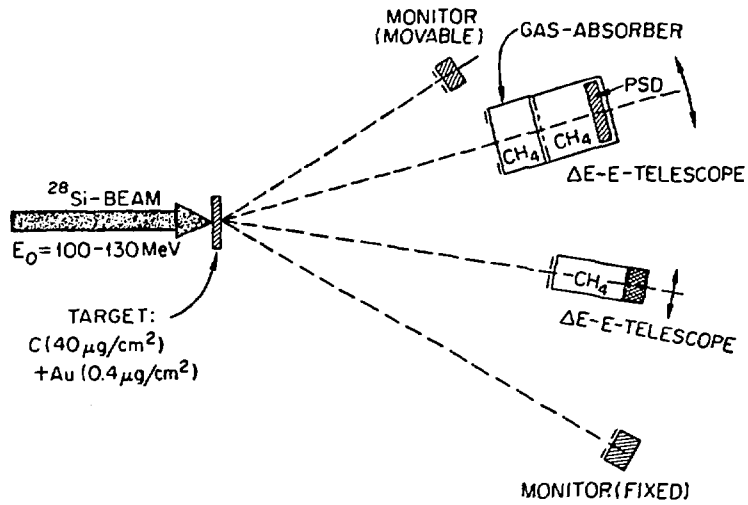
FIG. 2. Experimental setup. The gas used for the ionization chamber and
the absorber was isobutane (C_4H_{10}). The absorber gas was enclosed by two
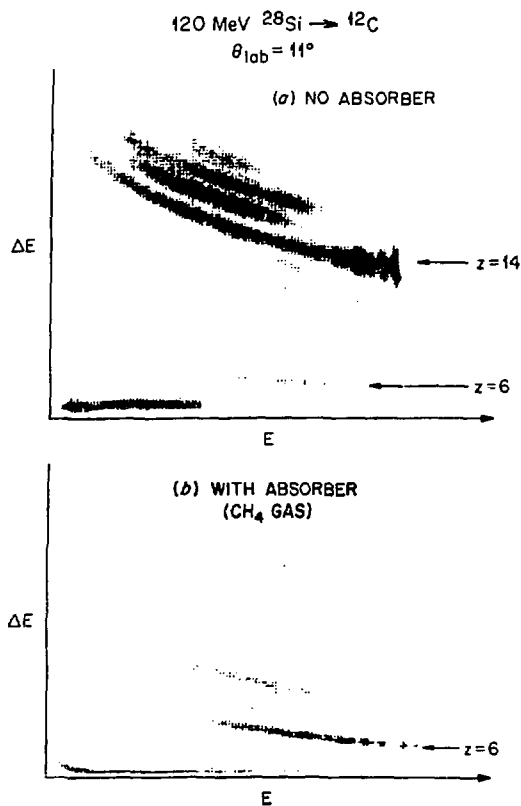0.001" thick mylar windows.

FIG. 3. Two dimensional
ΔE vs. E spectra with (b)
and without (a) absorber.

$^{12}C(^{28}Si,^{12}C)^{28}Si$
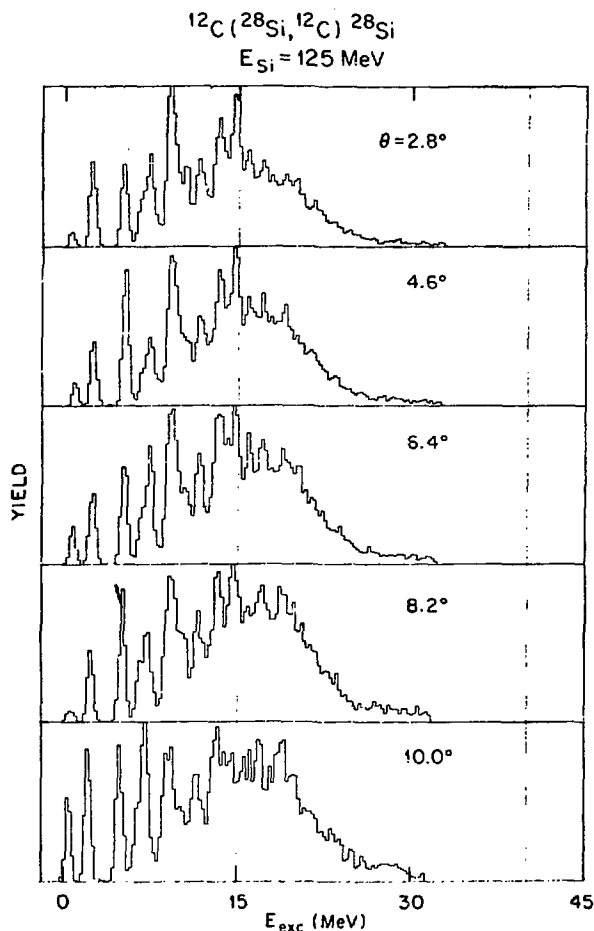$E_{Si} = 125$ MeV

FIG. 4. Carbon energy spectra from 125 MeV Si incident carbon target. The excitation energies appearing in the abscissa were calculated after correcting the measured energy for losses in the absorber and with the kinematics of $^{12}C(^{28}Si,^{12}C)^{28}Si$.

sensitive ΔE-E detector system. The measured energy spectra were corrected for energy loss in the absorber and then transformed to excitation energy using the kinematics of $^{12}C(^{28}Si,^{12}C)^{28}Si$ scattering to obtain the spectrum shown here. The energy resolution in the final spectrum is a few hundred keV and is limited by the silicon detector and the energy straggling in the absorber. Figure 5 shows similar spectra, though slightly compressed, for outgoing carbon, nitrogen and oxygen
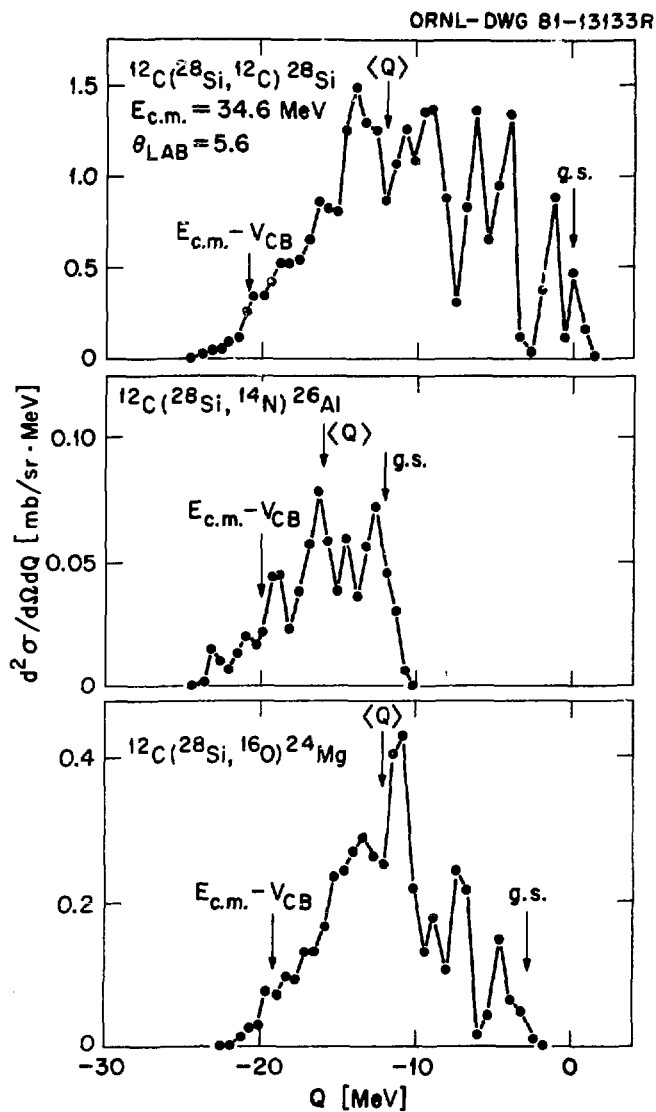
ORNL-DWG 81-13133R

FIG. 5. Q-value spectra for outgoing carbon, nitrogen and oxygen.
Calculated in the same way as the data in Fig. 3 but with a compressed scale.

nuclei. The Q values were calculated using two-body kinematics for the processes indicated in the figure.

While discrete lines at high and low excitation energies are clearly visible in these energy spectra, we do not intend to focus our attention on these individual transitions. As is evident from these figures the yield at backward angles, for the channels shown, is distributed around some large negative Q value. In the present analysis we consider only the first three moments of these Q value distributions and disregard the discrete lines in the spectrum. Figure 6 shows the most probable Q value (first moment) for two outgoing channels (carbon and oxygen)
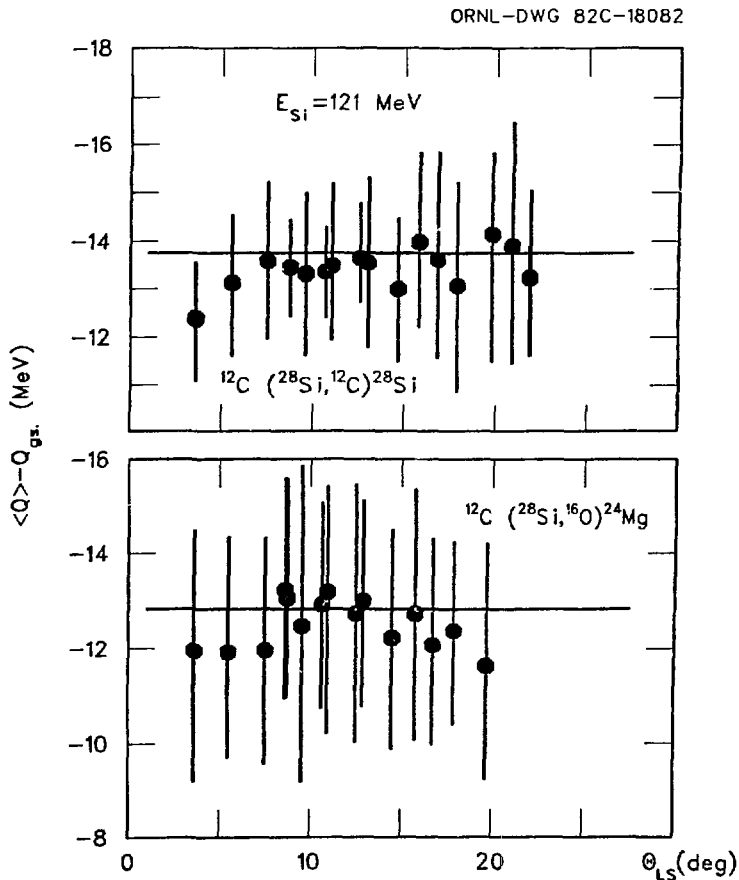
ORNL-DWG 82C-18082

FIG. 6. Dependence of the centroids of the measured Q-value distribution on the angle of observation.

measured at several scattering angles and at a single bombarding energy. The behavior seen here is a clear signature for the complete damping of the projectiles' kinetic energy. A large number of transitions to a continuum of overlapping states are involved but the centroid of the Q value distribution stays the same regardless of scattering angle. Similar effects have been observed for deep inelastic scattering in the collisions between heavier nuclei and attributed to orbiting.[1] We converted the total yield for each reaction channel to the center-of-mass system, using the measured most probable Q-value ($\bar{Q}$) to calculate the transformation Jacobian. The resulting center-of-mass angular distributions for the total yields of C, N and O are shown in Fig. 7. The angular distributions follow a $1/sin\theta_{cm}$ angular dependence, which indicates the long lifetime of the rotating complex. The behavior shown in Figs. 5, 6 and 7 prevails at all the bombarding energies that we studied (99 MeV $\leq E_{Si} \leq$ 133 MeV) and can be characterized as the decay of a rotating dinuclear complex formed in the collision. The most probable value of the total kinetic energy of the outgoing fragments is independent of the emission angle and the probability for scission at any given angle θ, given by $d\sigma/d\theta$, is independent of θ. A more quantitative analysis outlined below shows that the measured total kinetic energy of the fragments is determined by the magnitudes of the potential and centrifugal energies stored in the rotating complex.

In the study of strongly damped reaction products from collisions between light heavy ions the important role of the incoming orbital angular momentum in determining the total kinetic energy of the

ORNL—DWG 81—13134R2
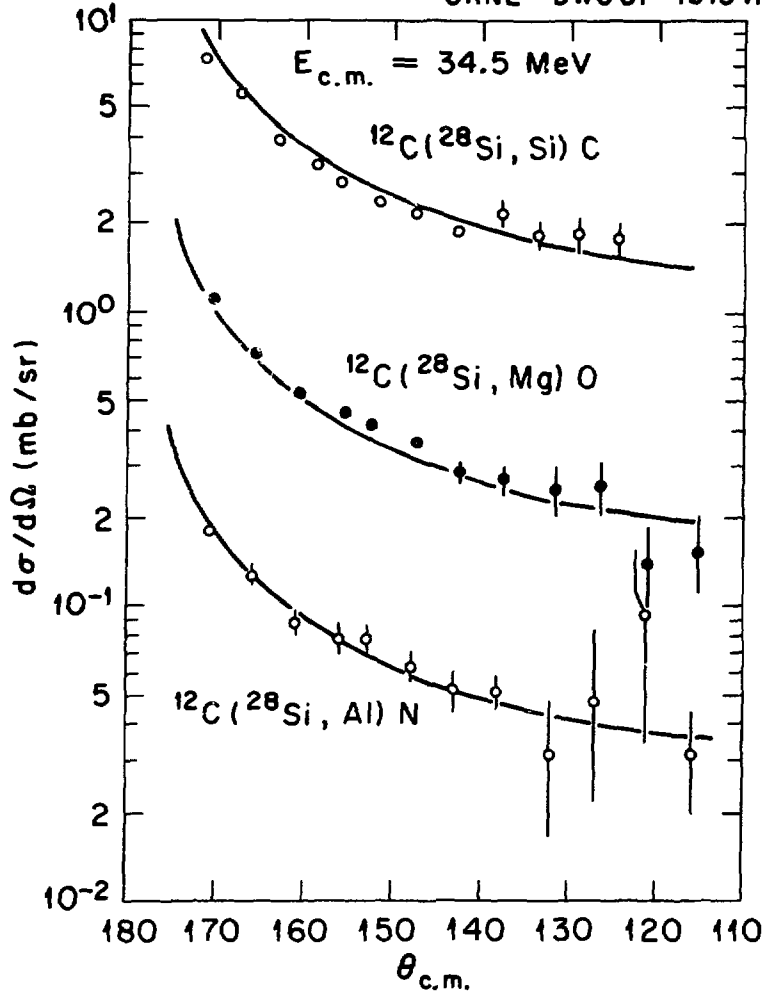
FIG. 7. Center-of-mass angular distributions for the total
reaction yield at backward angles for several exit channels.

fragments is well documented.[8,9,10] The total kinetic energy of com-
pletely damped products equals the energy stored in the rotating
dinuclear system, i.e. the combined nuclear, Coulomb and centrifugal
energies, prior to scission. The most probable Q value does not depend
on the angle at which the spectrum was measured and thus we can associate
a single most probable Q value ($\bar{Q}$) for a given reaction channel at each

bombarding energy. The resulting bombarding energy dependence of $\bar{Q}$ is shown in Fig. 8 for four outgoing channels. In all cases a linear fit
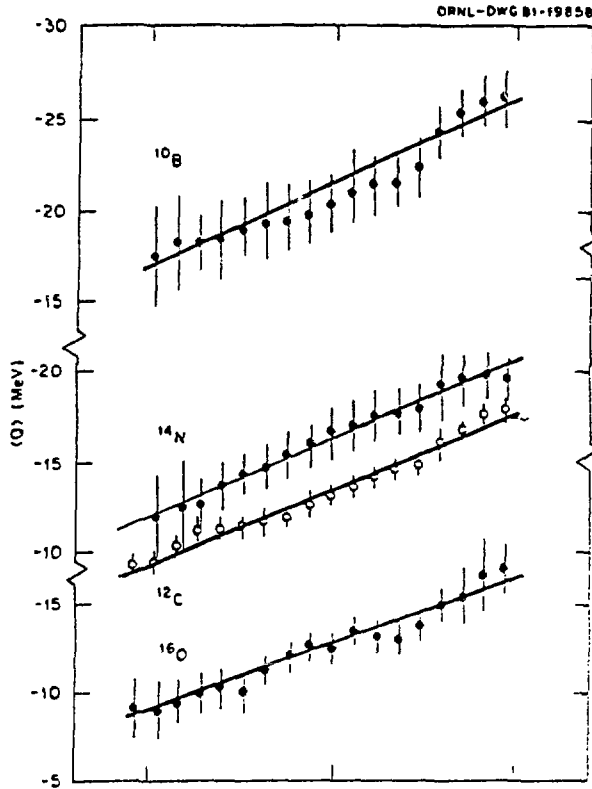

FIG. 8. The bombarding energy dependence of the centroids of the Q-value distribution for the reaction yield in the backward hemisphere for several final partitions.

provides a good description of the data but the slopes differ slightly from one channel to the other. As we shall see in the ensuing analysis such linear bombarding energy dependence arises from the centrifugal contribution to the energy stored in the relative dinuclear motion.

In our analysis and interpretation of the data we assume the formation and subsequent decay of a rotating dinuclear system (see Fig. 9). The total energy stored in the relative dinuclear motion is given by

$$E_{Kin}^{f} = V_{Nucl}(d) + V_{Coul}(d) + \frac{h^2 \ell_f(\ell_f+1)}{2\mu d^2} \tag{1}$$

ORNL—DWG 82-20622

$$E^f_{KIN} = \underline{\underline{a_0}} \qquad + \qquad \underline{a_1 \, E^i}$$

$$E^f_{KIN} = \underline{\underline{V_{COUL}(d) + V_{NUCL}(d)}} + \frac{\hbar^2}{2\mu d^2} \, \underline{\ell_f(\ell_f + 1)}$$
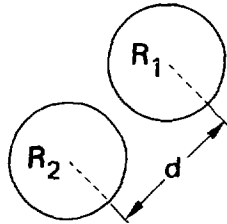
$$d = R_1 + R_2 + X$$

V_{COUL} (d) — CHARGED SPHERES

V_{NUCL} (d) — PROXIMITY TYPE (BASS)

$\ell_f = f * \ell_i$

ℓ_i = INCOMING ANGULAR MOMENTUM

FIG. 9. Quantities used in evaluating the kinetic energy available for products from the decay of an orbiting dinuclear complex.

d is defined along with other quantities in Fig. 9. ℓ_f is the orbital angular momentum of relative motion for the two nuclei in this rotating complex.

The results shown in Fig. 8 can be cast in a slightly different form by observing that the most probable value of the final kinetic energy available to the outgoing fragments (E^f_{Kin}) is directly related to the Q value by:

$$E^f_{Kin} = E_{cm} + \bar{Q} \qquad\qquad (2a)$$

The linear bombarding energy dependence seen in Fig. 8 can therefore be written in the form

$$E^f_{Kin} = a_0 + a_1 E_{cm} \tag{2b}$$

The experimental values deduced for a_0 and a_1 appear in table I.

TABLE I

$$E^{Kin}_f = a_0 + a_1 \cdot E^{c.m.}_i$$

Channel	a_0 (MeV)	a_1
B + P	9.8 ± 3	0.15 ± 0.05
C + Si	16.7 ± 2	0.12 ± 0.03
N + Al	12.1 ± 1	0.19 ± 0.05
0 + Mg	11.8 ± 3	0.30 ± 0.09

Equations (1) and (2) both express the dependence of the fragment's total kinetic energy on the bombarding energy. Neglecting any dependence of the nuclear and Coulomb potentials on bombarding energy enables us to identify

$$a_0 = V_{Coul}(d) + V_{Nucl}(d) \quad . \tag{3}$$

For local potentials with all other parameters, except for d, fixed, Eq. (3) can be used to derive the nuclear separation at scission - d.

For the Coulomb potential, $V_{Coul}(d)$, we take the form derived for two point charges, while V_{Nucl}, the nuclear potential, is a proximity potential with parameters determined by R. Bass from fits to a large body of fusion data.[11] Equation (3) leads to a single value of d for each channel and the resulting radii are shown in table II where we also

TABLE II

Channel	$d = R_1 + R_2 + X$	X
B + P	7.1 ± 0.5	2.1
C + Si	8.2 ± 0.2	3.2
N + Al	7.2 ± 0.3	2.0
O + Mg	7.0 ± 0.3	1.7

list the quantity $X = d-R_1-R_2$ which is the distance between the half density surfaces of the two nuclei. The values of R_1 and R_2 are half density radii determined from systematics[11,12] ($r_0 \lesssim 1$). The values of d vary between 7 and 8 fermi for the exit channels that we studied. For all these channels the value of d is in the vicinity of the "fusion barrier" i.e. the radius at which the combined nucleus-nucleus potential has reached a maximum value. Note that the channels involving greater transfer of charge are associated with smaller values of X and therefore, presumably, larger spatial overlap.[13]

We now turn our attention to the parts of the expressions (1 and 2) for the total kinetic energy of the fragments that depend on the bombarding energy. Equating the slopes of Eq. (1) and Eq. (2b) we get

$$a_1 = \frac{d}{dE_{cm}} \frac{h^2 \ell_f(\ell_f+1)}{2\mu d^2}$$ (4)

μ is the reduced mass and d is the radius parameter determined from the analysis of the energy independent part as outlined above. ℓ_f is the orbital angular momentum of relative motion for the two nuclei in the rotating complex. The relationship between this angular momentum (ℓ_f) and the asymptotic value of the angular momentum in the entrance channel (ℓ_i) can be cast in the form

$$\ell_f = F \ell_i \qquad (F \leq 1)$$

Approximations for the factor F can be derived from classical mechanics and they are shown in Fig. 10. F can be called a "clutching factor" whose value depends on the geometry of the rotating objects and also on whether they rotate as a rigid dumbbell (sticking), roll on top of each other, or just slide around each other (F = 1). One should note that the rolling formula shown in Fig. 10 reduces to the commonly used value of F = 5/7 only when $R_1 = R_1'$ and $R_2 = R_2'$ i.e. the case of two spheres in contact ($\sim$ overlap at the half density radius). Equation 4 can now be rewritten as an expression for this clutching factor F

$$F^2 = a_1 \cdot \frac{2\mu d^2}{h^2} / \frac{d}{dE_{cm}} [\ell_i(\ell_i+1)]$$ (5)

For the nucleus-nucleus separation parameter-d the values in table II can be used and a_1 obtained from a linear fit to the data. The largest uncertainty in evaluating F from the above expression comes from our lack of a precise knowledge of the incoming angular momentum trajectory

ORNL–DWG 82-20621
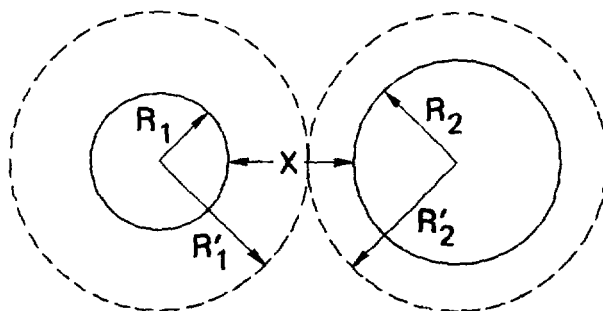
$$d = R_1 + R_2 + X = R'_1 + R'_2$$

$$f \equiv L_{final}/L_{initial}$$

STICKING $$f = \frac{\mathcal{L}_{12}^{final}}{\mathcal{L}_{12}^{final} + \mathcal{L}_1 + \mathcal{L}_2}$$

ROLLING $$f = \frac{\mathcal{L}_{12}^{final}}{\mathcal{L}_{12}^{final} + \dfrac{\mathcal{L}_1 \mathcal{L}_2 \, d^2}{\mathcal{L}_1 \, R'^2_2 + \mathcal{L}_2 \, R'^2_1}}$$

FIG. 10. Expressions for the orbital angular momentum of a rotating dinuclear complex. R_1 and R_2 are the nuclear half density radii (typically — ~ 1.0 x $A^{1/3}$) and R'_1 R'_2 are the radial distances to the pivotal point of the rotating complex. $\mathscr{I}_{2,1} = 0.4 \, MR_{2,1}^2$ are the individual moments of inertial and $\mathscr{I}_{12} = \mu d^2$.

$\ell_i = \ell_i(E)$. All we can do at this stage is put limits on this quantity by postulating that the contributing trajectories come from the region bounded by the grazing angular momentum on the high side and by the critical angular momentum (ℓ_c) for fusion on the low side. The grazing angular momenta were determined using the $^{28}Si + {}^{12}C$ optical model potential determined by Satchler et al.[14] The critical angular momenta were determined by using a sharp cutoff approximation for the fusion cross section; namely assume that $\sigma_{fus} = \pi\lambda^2 \ell_c(\ell_c+1)$. Our own fusion data, measured during the same experiment, as well as the data of Lesko et al.[15] were used to obtain values of ℓ_c with that expression. A summary of the results is shown in Fig. 11. In general the data are consistent with our assumption of a rotating complex but not very useful for determining whether the orbiting nuclei slide, roll or stick. Note that as the mass asymmetry between the orbiting nuclei increases so does the difference between the rolling and sticking factors. We hope that similar measurements in systems with larger asymmetry can be used for resolving the two possibilities. In summary the large body of data I have shown so far as well as similar data on several other systems can be successfully described by postulating the formation of a long-lived rotating dinuclear complex at an early stage of the collision, and its subsequent decay to the observed exit channels.

Before we examine the data obtained at higher bombarding energies several unanswered questions have to be addressed. In the measurements presented so far only the nuclear charge of the detected particles was determined. The relative role of the isotopes other than ^{12}C and ^{16}O in
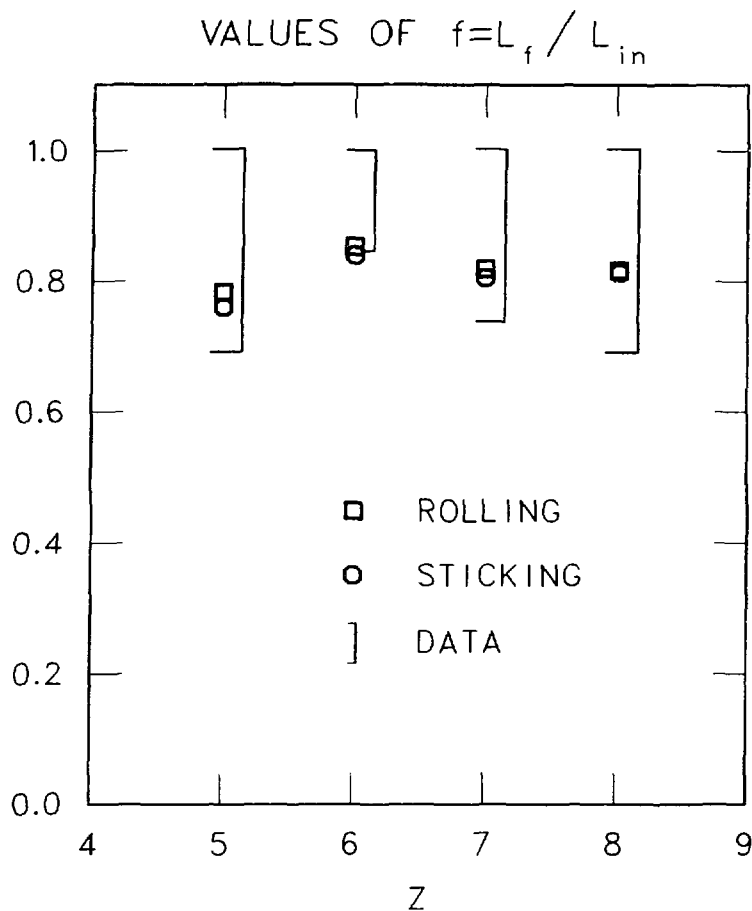
VALUES OF $f = L_f / L_{in}$

FIG. 11. The reduction factor of the asymptotic angular momentum — comparison of classical calculation and experimental results.

the C and O channels was not determined experimentally. We therefore studied the same reaction $^{28}Si + ^{12}C$ at a bombarding energy of 135 MeV (a higher bombarding energy than any shown so far) and identified the mass and charge of the products. The recoiling C, N and O isotopes were detected and identified with a large heavy ion hybrid detector system[16] at the focal plane of the Holifield Laboratory's Enge

Split-Pole Spectrograph. Our data at this bombarding energy of 135 MeV show that the combined ^{13}C and ^{14}C yield amounts to less than 5% of the total C yield (all isotopes combined) and similar results apply also to the isotopic yields of oxygen.

A second question relates to the possibility that the observed yield, or a large part of it, especially·in the continuum region, does not stem from the two-body process that we assumed, but, is a result of some multiple step evaporation process of a completely different nature. We have therefore carried out a coincidence experiment in which both of the fragments (or their decay products after evaporation) that would be produced in such a two-body process were detected.

The arrangement used in the experiment is shown in Fig. 12. On one

ORNL-DWG 82-20724

^{28}Si ON ^{12}C COINC. EXPERIMENT

FIG. 12. The experimental arrangement used in the coincidence measurement.

150 MeV ^{28}Si

^{12}C
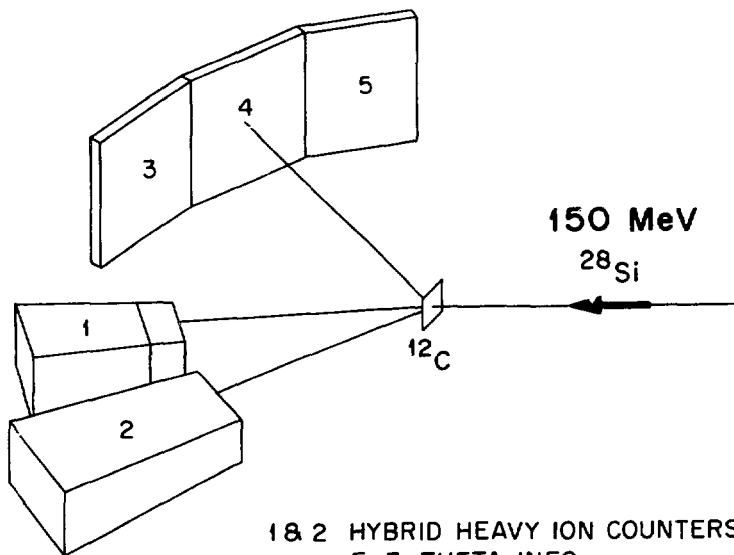
1 & 2 HYBRID HEAVY ION COUNTERS E, Z, THETA INFO.

3 & 4 & 5 X AND Y POSITION SENSITIVE PARALLEL PLATE AVALANCHE COUNTERS THETAX, THETAY, TIME INFO. (ONLY Z > 2)

side of the beam a battery of gas filled ΔE-E telescopes were used to determine the charge and the energy of the detected particle and define a reaction plane. On the opposite side of the beam an array of three large area x, y position sensitive parallel plate avalanche counters were mounted in such a way that their active areas covered a large angular range below, above and in the reaction plane. The bias voltage of the avalanche counters was set low enough so that they would not trigger on energetic light particles, and therefore only heavy particles (Z > 3) were detected. The analysis of these data is fairly complex and still underway.[17] Figure 13 shows some results of a preliminary analysis of these data. Shown
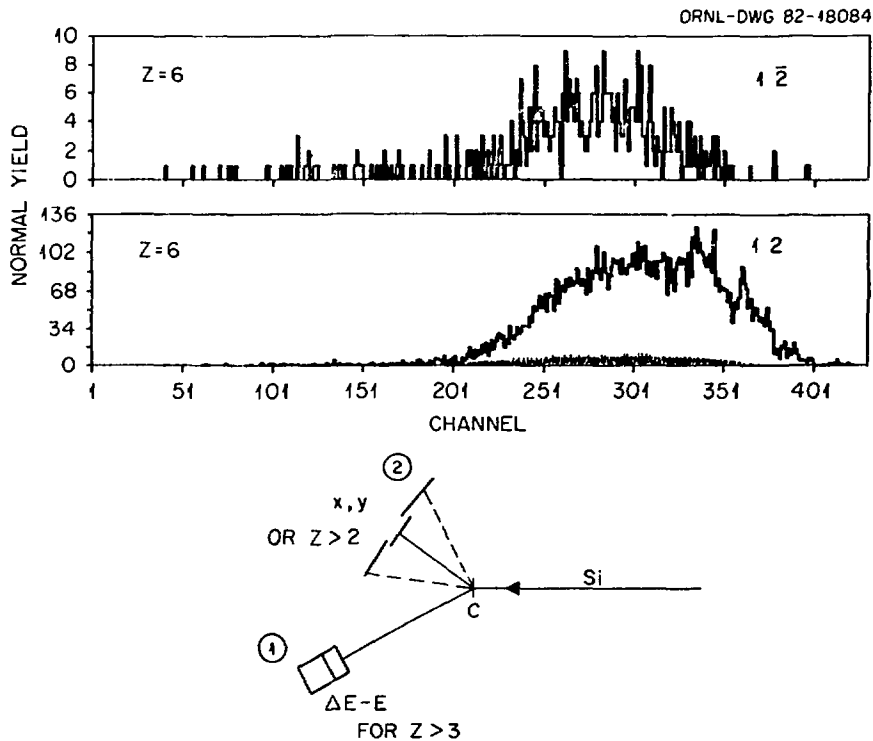

FIG. 13. Preliminary results from coincidence experiments.

are two Z = 6 (carbon) spectra measured in the same ΔE-E detector on one side of the beam under two conditions: The upper part of the figure shows the carbon ions detected with no associated (heavy) particle hitting any of the avalanche counters on the opposite side of the beam. The lower part of that figure shows the same spectrum accumulated for cases in which there was an associated "hit" in the avalanche counters. It is clear that a quantitative analysis must await more complete reduction of the data but qualitatively the claim can be made that most of the detected carbon nuclei have some associated particle (heavier than α particles) emitted to the opposite side of the beam. That is, the detected carbon isotopes originate from two-body like processes, such as inelastic scattering or possibly transfer followed by successive evaporation.

It is not expected that the linear dependence on bombarding energy that is extracted from the measured inclusive energy spectra, in the way we have done so far, will continue unchanged to higher energies. For some incident energy the total excitation energy reached in the exit channel will be so high that both fragments will emerge so highly excited that they will <u>both</u> decay in flight. In the $^{12}C + ^{28}Si$ exit channel, for example, the ^{12}C nucleus if excited beyond ~ 10 MeV (α threshold + Coulomb barrier for α decay) will decay in flight and not reach the counter. At this point, i.e. at a bombarding energy where the ^{12}C nucleus has a high probability of being highly excited, the observed Q value dependence, based on the measured energy spectra, will show a much slower rate of increase with bombarding energy. The actual bombarding energy where this downturn in the linear dependence of $\bar{Q}$ on E_{cm} will

occur depends on the relationship between the most probable Q value and the bombarding energy (see Fig. 8 and table I) and on the way in which this excitation energy is divided between the ^{12}C and ^{28}Si nuclei. The latter question concerning the division of excitation energy between the fragments remains a topic of controversy.

We have therefore continued, in a subsequent experiment, the singles measurements to higher bombarding energies. The new data measured between 125 and 190 MeV bombarding energy have many of the features that were observed for the lower energy data, namely complete damping of the kinetic energies (independent of angle), $1/\sin\theta_{cm}$ angular distribution and a linear dependence of the centroids of the Q value distribution ($\bar{Q}$) on the bombarding energy. Figure 14 shows energy spectra for carbon

ORNL-DWG 82-19208
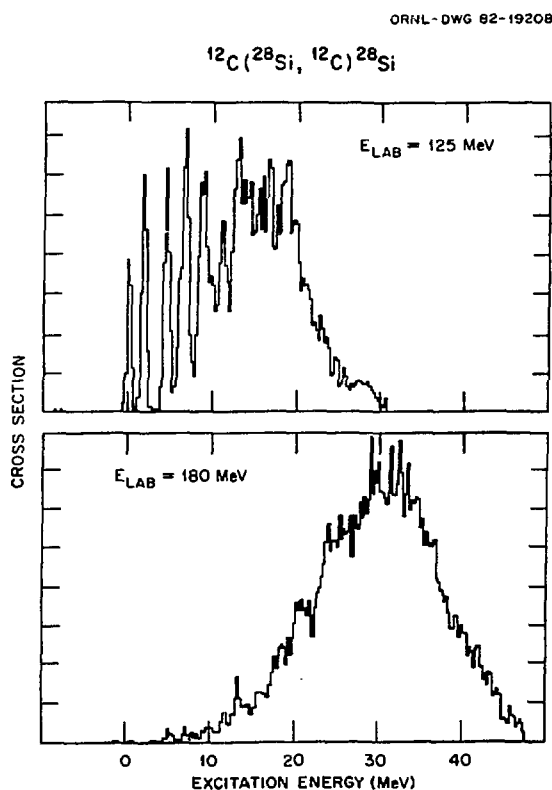
$$^{12}C(^{28}Si, \, ^{12}C)^{28}Si$$

FIG. 14. Energy spectra for carbon isotopes.

isotopes measured at 125 MeV and 180 MeV bombarding energy. A shift of
about 15 MeV in the centroid of the Q value distribution with only a
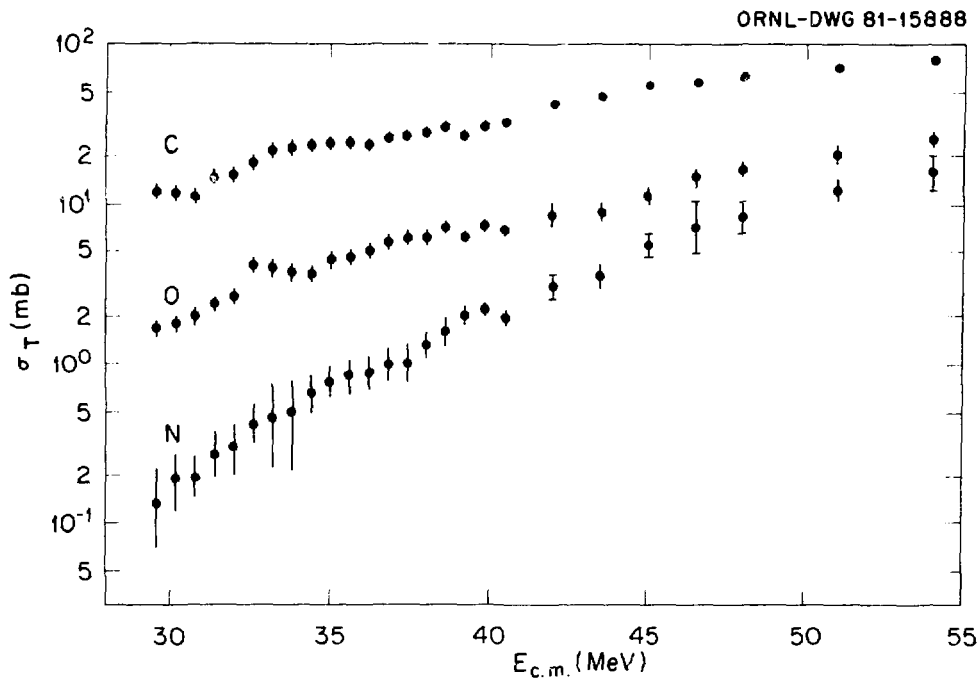slight increase in its width is apparent. Figure 15 shows the total

ORNL-DWG 81-15888

FIG. 15. Integrated cross section for the orbiting yield:
$1/\sin\theta_{cm}$ angular distribution is assumed also for the forward
hemisphere.

cross section for this process integrated from 0° to 180° with the
measured $1/\sin\theta$ angular dependence. The region in Fig. 15 with the
closely spaced data points corresponds to the earlier measurements that I
have already discussed and the more sparsely spaced data points are from
the newer measurements at higher energies. A steady increase of the
cross sections can be seen but one should note that the cross section for
the oxygen channel remains about a factor of five below the measured car-
bon channel cross sections even at the highest bombarding energies. We

see from this figure that the cross section for the orbiting process
reaches 100 mb at the highest energy shown here $(E_{si} = 180 \text{ MeV})$. Most
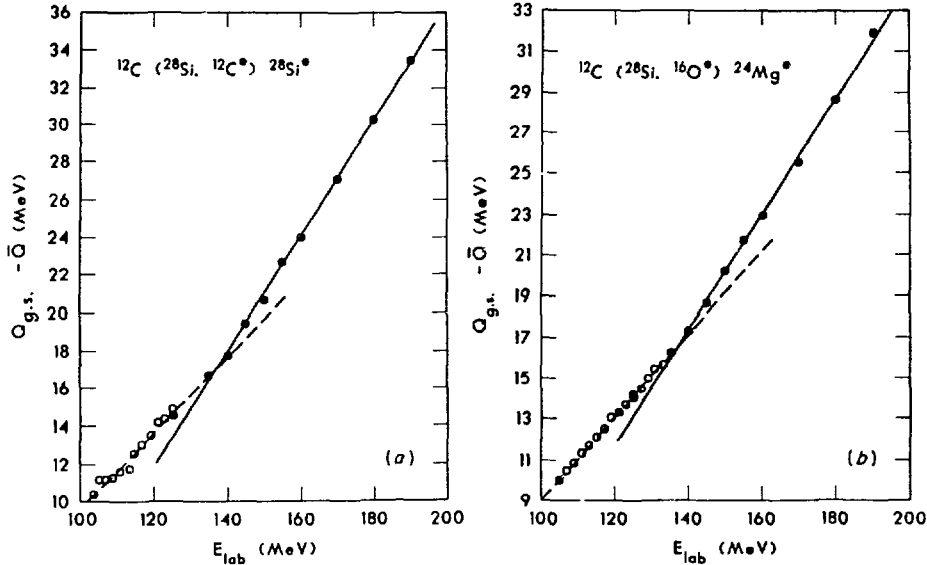interesting however is the result shown in Fig. 16. Here we see that the

FIG. 16. Dependence of most probable $\bar{Q}$ value $(Q-Q_{gs})$ on
bombarding energy for the O + Mg channel (b) and C + Si
channel (a).

linear dependence of $\bar{Q}$ on bombarding energy takes a sharp __upturn__ (rather
than the expected downturn). This is shown for both the oxygen and the
carbon channels. One can see that the slopes for the C and the O chan-
nels are identical in the high energy region. Figure 17 presents the
same results (shown here for the carbon channel only) in a different plot
showing the final kinetic energy of the fragments $(E_{cm} + \bar{Q})$ as a function
of bombarding energy. There is a clear flattening out of the energy
dependence. The simplest explanation for such behavior is quite
obvious; the angular momentum of the rotating dinuclear complex stopped
increasing as a function of bombarding energy. Such behavior is expected
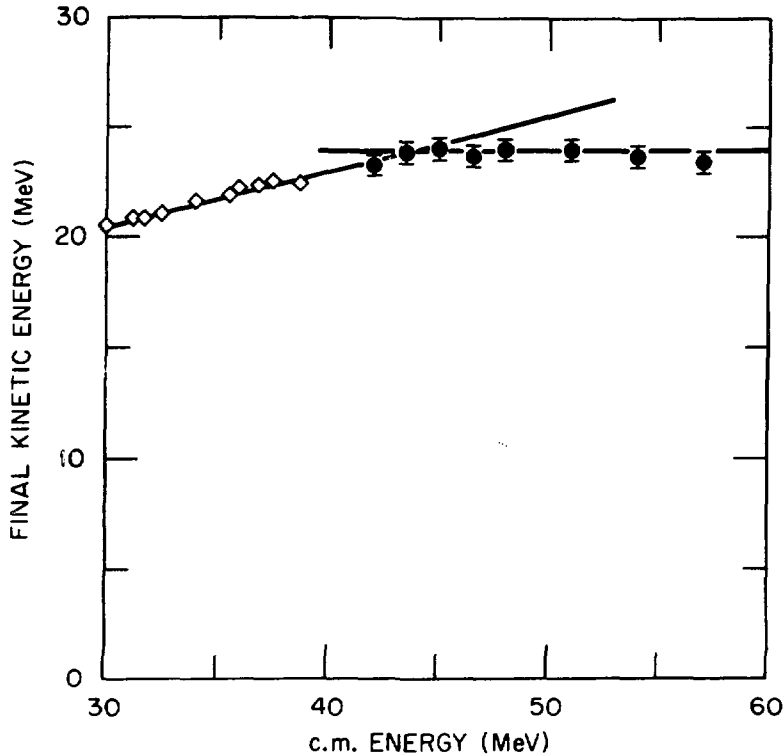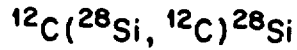
ORNL-DWG 82-19207

$$^{12}C(^{28}Si, ^{12}C)^{28}Si$$

FIG. 17.
The dependence
of the final
kinetic energy
of outgoing
C + Si on
bombarding
energy.

once the angular momenta ℓ_f of the orbiting complex reaches a critical

value for which the nuclei no longer experience attraction at contact

(i.e. the "pocket" in the combined nucleus nucleus potential

disappears). Under such circumstances partial waves with angular momenta

higher than this critical value (ℓ_c) can not be trapped into a rotating

complex for any period of time and therefore the flux associated with

them cannot contribute to the orbiting process. The limitation postu-

lated here for orbiting is of the same nature as the limits on angular

momenta leading to fusion postulated in the one dimensional model of Bass.[11] Furthermore a calculation of the critical angular momentum for $^{12}C + ^{28}Si$ with the potential parameters given by Bass[11] yields a critical angular momentum of $\ell_f \sim 22-23$, which sets in at an incident energy of $E_{cm} = 45$ MeV when the two nuclei roll on top of each other or at $E_{cm} = 52$ MeV in the sticking limit. There is obviously a close relationship between the behavior seen here for the orbiting process and the angular momenta limiting the fusion of the two nuclei.

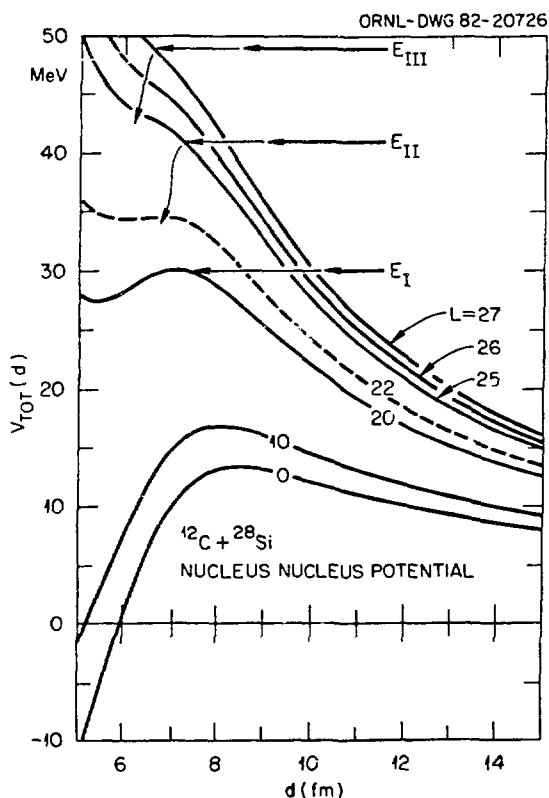The one dimensional model for fusion outlined by R. Bass postulates that the flux associated with a given partial wave ℓ_i will go to fusion if two conditions are satisfied. First, the nuclei must surmount their mutual Coulomb and centrifugal barrier (= the fusion barrier) and second, an attractive force must be in effect beyond the top of the barrier, i.e., the nucleus-nucleus potential must have a pocket. At low energies (region I in Fig. 18) these conditions are readily fulfilled and fusion overwhelmingly dominates ($E < E_I$ in Fig. 19). At higher energies ($E_{III} > E > E_{II}$) the total potential for the grazing partial wave does not have a pocket any

ORNL-DWG 82-20726

FIG. 18. The $^{12}C + ^{28}Si$ nucleus-nucleus potential. The radius and other parameters for the nuclear potential are from reference 11.
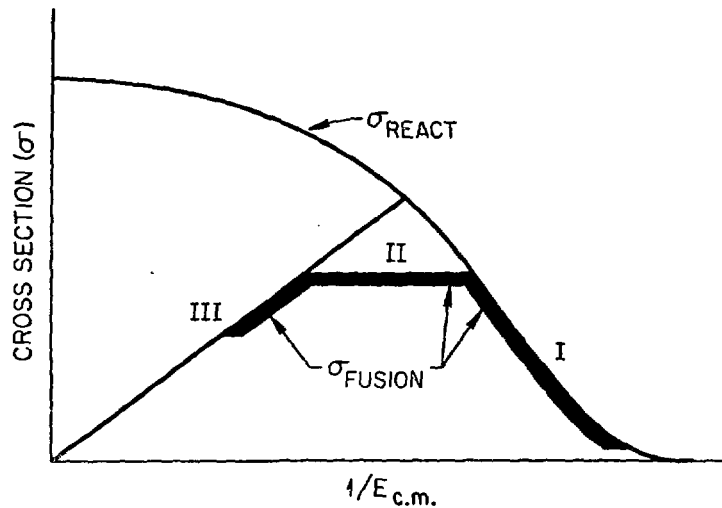
ORNL-DWG 82-20725

FIG. 19. Schematic description of the bombarding energy
dependence of fusion cross section.

more. At this point there would be no fusion except for the fact that

the incident nuclei can be excited and lose some of their orbital

angular momentum. Then, as long as the nucleus-nucleus potential for

the reduced orbital angular momentum has a pocket, the nuclei can

fuse. What we find in our analysis is that even though the two precon-

ditions for fusion are satisfied the nuclei do not necessarily fuse but

instead they can rotate a while around each other and then be emitted.

This "escape-probability" is reflected in the magnitude of the cross sec-

tions in Fig. 15. (At forward angles the yield of fully damped reaction

products rises more steeply than $1/sin\theta$ and we therefore feel that the

values given in Fig. 15 are a lower limit for the magnitude of the

orbiting cross section.) The magnitude of the fusion cross section,

therefore, follows the heavy line shown in Fig. 19. The reduction in

fusion cross section seen in region II has also been described by adding

one more requirement in addition to the two preconditions leading to fusion.

These take the form of requiring the nuclei to reach some critical distance before they can fuse[18] or the requirement of a non zero inward radial velocity at the top of the barrier (an "extra push"[19-20]).

We have shown here by a careful examination of reaction products emitted in the backward hemisphere that the energy and angular distributions as well as the bombarding energy dependence of these products result from the formation of a rotating dinuclear system at the early stages of the collision and its subsequent decay.

It must be recognized that the shapes of the angular distributions and the energy spectra for products associated with this orbiting process are identical with those expected from a process in which the complete amalgamation of target and projectile (fusion) is followed by fission into two large fragments. The only arguments for invoking this different process (orbiting) to explain such data stems from the fact that the measured cross sections are much larger than those expected for the fis ion of light nuclei with A < 80. In addition the relationship to deep-inelastic scattering seen in heavier systems, and also at forward angles in collisions between lighter heavy ion, is appealing.

References

1. J. Wilczyński, Phys. Lett. 47B, 484 (1973).

2. D. Shapira, J. L. C. Ford, Jr., J. Gomez del Campo, R. G. Stokstad and R. M. DeVries, Phys. Rev. Lett. 43, 1781 (1979).

3. D. Shapira, D. DiGregorio, J. Gomez del Campo, R. A. Dayras, J. L. C. Ford, Jr., A. H. Snell and P. H. Stelson, "Fusion and Peripheral Processes in the Collision of ^{20}Ne + ^{20}Ne and ^{20}Ne + ^{16}O," to be published.

4. D. Shapira, R.Novotny, Y. D. Chan, K. A. Erb, J. L. C. Ford, Jr., J. C. Peng and J. D. Moses, Phys. Lett. 114B, 111 (1982).

5. D. Shapira, J. L. C. Ford, Jr., J. Gomez del Campo and P. H. Stelson, Phys. Rev. C 21, 1824 (1980).

6. R. Eggers, M. N. Namboodiri, P. Gonthier, K. Geoffroy and J. B. Natowitz, Phys. Rev. Lett. 37, 324 (1976). J. B. Natowitz, M. N. Namboodiri, R. Eggers, P. Gonthier, K. Geoffroy, R. Harris, C. Towsley and K. Dos, Nucl. Phys. A277, 477 (1977).

7. A. Glaesner, "A Study of Orbiting in ^{12}C + ^{24}Mg," Diplom. Thesis, May 1982, Technische Universitat Munchen.

8. T. Cormier, P. Braun-Munzinger, P. Cormier, J. W. Harris and L. L. Lee, Jr., Phys. Rev. C 16, 215 (1977).

9. P. Braun-Munzinger, T. M. Cormier and C. K. Gelbke, Phys. Rev. Lett. 37, 1582 (1976).

10. R. R. Betts and S. B. DiCenzo, Phys. Rev. C 19, 2070 (1979).

11. R. Bass, Phys. Rev. Lett. 39, 265 (1977).

12. A. D. Myers, Nucl. Phys. A204, 465 (1973).

13. M. H. Simbel and A. Y. Abul-Magd, Z. Phys. A294, 277 (1980).

14. G. R. Satchler, M. L. Halbert, R. G. Stokstad, R. M. DeVries, D. A. Goldberg and J. G. Cramer, Nucl. Phys. A346, 179 (1980).

15. K. T. Lesko, K. K. Lock, A. Lazzarini, R. Vandenbosch, V. Metag and H. Doubre, Phys. Rev. C 25, 872 (1982).

16. D. Shapira, G. L. Bomar, J. L. C. Ford, J. Gomez del Campo and L. C. Dennis, Nucl. Instrum. and Methods 169. 88 (1980).

17. R. Novotny et al., to be published.

18. D. Glas and U. Mosel, Phys. Lett. 49B, 301 (1974).

19. J. R. Nix and A. J. Sierk, Phys. Rev. C 15, 2072 (1977).

20. W. J. Swiatecki, Nucl. Phys. A376, 275 (1982).